The Pennsylvania State University

The Graduate School

College of Engineering

ACOUSTICALLY ACTUATED MICROSTRUCTURES

A Thesis in

Engineering Science and Mechanics

by

Murat Kaynak

Submitted in Partial Fulfillment
of the Requirements
for the Degree of
Master of Science

August 2016

The thesis of Murat Kaynak was reviewed and approved* by the following:

Tony J. Huang
Professor of Engineering Science and Mechanics
Thesis Advisor

Bernhard R. Tittmann
Schell Professor of Engineering Science and Mechanics

Corina S. Drapaca
Associate Professor of Engineering Science and Mechanics

Judith A. Todd
Professor of Engineering Science and Mechanics
P.B. Breneman Department Head

*Signatures are on file in the Graduate School

ABSTRACT

Acoustic has been an attractive technique for microfluidic applications in biomedical, physical and chemical field due to its noninvasive, harmless and contactless actuation. On the other hand, microfabrication using UV-light is an interesting method since it provides easy, inexpensive and single-step fabrication. In this thesis, integration of microfabrication and acoustic actuation has been demonstrated in order to combine advantages of both techniques for biomedical engineering applications.

First, in situ fabricated and acoustically actuated microrotors are illustrated. A polymeric microrotor with sharp-edge structures is fabricated in situ by applying a patterned UV light to polymerize a photocrosslinkable polyethylene glycol solution inside a microchannel around an existing polydimethylsiloxane axle. To actuate the microrotors by oscillating the sharp-edge structures, we employ piezoelectric transducers which generate tunable acoustic waves. The resulting acoustic streaming flows rotate the microrotors. A 6-arm microrotor could exceed 1200 revolutions per minute.

Second, acoustic actuation of biologically mimicked and flagellated microswimmers is developed. Microswimmers are in situ fabricated by using UV light in a microchannel fulfilled with a photocrosslinkable solution. When acoustic waves are applied, the flagella of microswimmers oscillate, which, in turn, move them either rotationally or directionally depending on their design. The rotational and directional movements of these biologically mimicked microswimmers are tuned by pick-to-pick voltage through a transducer. A directional flagellated microswimmer could exceed a velocity of 1200 μm per second at 160 V_{PP}, which is much faster than many biological

counterparts such as bacteria, while rotational micrswimmers can exceed 200 RPM. Simple microfabrication as well as remote actuation via acoustic waves is promising for microapplications such as microdrilling, targeted drug delivery and microsurgery in biomedical, chemical and biological engineering.

TABLE OF CONTENTS

LIST OF FIGURES

ACKNOWLEDGEMENTS

I would like to express my deepest gratitude to my advisor, Dr. Tony J. Huang, for providing me with this research opportunity, guiding my study and encouraging me to do my best throughout my Master's education. His knowledge, enthusiasm and guidance have enable me to do independent research and to make my research ideas reality.

I would like to thank to Dr. Vincent Crespi and his group members, Paul Lammert and Amir Nourhani, for guiding my research theoretically along with suggestions. Discussions with them on the theory of my research was beneficial. Their careful and detail-oriented recommendation contributed a lot to my research.

I would also like to acknowledge Turkish Ministry of Education for supporting me financially. Their professional and friendly approach allowed me to focus on my study and do an exceptional research.

I would like to extend my appreciation to my mentor and close friend, Adem Ozcelik, for his never-ending academic and social support. I will never forget our productive academic discussions and his guidance on finding solutions to the problems that I encountered in my research and coming up with new ideas to further my research. I am sure of his academic knowledge and approach to science will make him a prominent scientist.

Lastly, I would like to thank to my mom Ayse Kaynak, my dad Sahin Kaynak and my siblings Mustafa Kaynak and Seref Kaynak. Their unconditional love and infinite support have always reminded me that success in academia is the result of not only doing research in the lab but also having an invaluable family.

DEDICATION

I dedicate my research to my grandparents, Sahan and Zuhtu Kaynak, who passed away years ago.

Chapter 1

1.1 Introduction

Microfluidics is an integration of science and engineering comprising of formulation and design of devices in small scale from millimeter to micrometer. Devices which are used in microfluidics are called microchips. Being small has allowed the microfluidics become lab-on-chip rather than chip in the lab. Smallness brings the advantage of using less material, less energy and, in turn, less expensive tools in both laboratories and engineering applications.[1–5]

Acoustics, which uses sound waves, is a contactless technique to manipulate objects not only in macroscale but also in microscale. The waves can be generated via several transducers such as piezoelectric transducers (PZTs) and inter digital transducers (IDTs) which generate different form of vibrations and waves. The response of materials and cells are able to be resulted in cell manipulation and acoustic driven of mechanical design.[5]

The ratio of inertial forces to viscous is named as Reynolds number (Re) which is a dimensionless quantity.[6–8] Re is used to characterize the fluid flow.

$$\mathrm{Re} = \frac{\text{inertial forces}}{\text{viscous forces}} = \frac{\rho v^2 L^2}{\mu v \mathrm{L}} \qquad 1\text{-}1$$

where ρ, ν, L and μ are the density of the fluid (kg/m^3), the kinematic viscosity (m^2/s), a characteristic linear dimension (m) and the dynamic viscosity of the fluid (kg/(m·s)), respectively. When Re is big, the inertial forces are dominant. For instance, a human has a

Reynolds number of ~10^4 while it is ~10^2 for a gold fish. When the dimension of devices are small enough, the life in microchips has its own rules such as low Reynolds number which could be less than 1 for microorganisms. In small scale, moving in a liquid is comparably difficult than moving in macroscale and requires relatively more power since the fluid acts as it is more viscous.[9]

1.2 Problem Statement

Remotely powered and autonomous micromotors play an important role in microelectromechanical systems (MEMS),[10–13] biomedical engineering,[14–19] and biochemical applications.[20,21] They are used in lab-on-a-chip applications for mixing[22,23] and pumping,[24,25] or for studying the rheological properties of microdroplets or microparticles.[26,27]

In recent years, significant advances have been made in actuating microstructures by hydrodynamic force,[28] laser manipulation,[29,30] bacterial motion,[31–33] magnetic force,[15,23] chemical propulsion,[34,35] and acoustic waves.[36–38] Yue et al. fabricated laser-actuated microgears with rotation rates around 60 revolutions per minute (RPM) at 2 watts.[29] Their method enabled simple in situ fabrication of microstructures in various geometries inside microchannels. Applying laser for actuation provides precision but simultaneous manipulation of microgears would require multiple laser beams. Moon et al. fabricated polymer micromachines that rotate around a pre-fabricated micropillar driven by hydrodynamic force.[28] A fluid is injected in the micro channel and a rotation rate of 5 RPM per 1 μL/min of fluid flow in a 200 μm wide channel is obtained. Leonardo et al.

studied micromotors that use bacteria as a source of driving force.[32] These micromotors could rotate at 1 RPM with an unstable frequency. Lu et al. and Ahn et al. utilized magnetic actuation for micromixing[23] and micropumping,[15] which require magnetic components and relatively complex operational setups. Shilton et al. introduced micromotors driven by surface acoustic waves[36,37] and obtained high rotation rate which opens new possibilities in micromanipulation.

Microswimmers have grabbed attention of scientists due to their practical and potential applications in small size.[38–46] Microswimmers which have contactless actuation are appropriate for many applications such as targeted drug delivery, particle separation, mixing, pumping, assembly, manipulation, microsurgery and chemical analysis by mimicking their biological counterparts such as bacteria. [23,47–55]

Mimicking the biological microswimmers is a reasonable method to design artificial microswimmers in order to take advantage of natural orientation of biology.[16,47,52,56–58] Depending on the medium where biological microswimmers live, the flagella have been evaluated both experimentally and numerically to be rotated helically, spirally and wave sinusoidally.[8,9,43,59–62] Their design which enables them to move in biological medium at low Reynolds number in microscale has been inspiring researchers to create decent artificial microswimmers.[9] Biological self-propelled microswimmers such as Escherichia coli (E. coli), human sperm, Chromatium okenii, Spirillum volutans and scallop have mechanisms to swim at low Reynolds number.[16,44,51,56,60,63,64] Their tails, the flagella, propel and steer these microorganisms by oscillation in several form and these movements in turn enable the microorganisms to be motile to find their food, reproduce and move to safer place.

Microswimmers can autonomously propel utilizing various energy types such as electrical, chemical, magnetic, acoustic and dual combination of them.[23,34,38,41,45,46,48,50,59,65–70] By inducing an external electric field, polarization of microswimmers creates chemical reaction and in turn motility of microswimmers between anode and cathode. The velocity can be adjusted by tuning the applied voltage. Chemical microswimmers utilize chemicals such as hydrogen peroxide as fuel to power the microswimmers. Chemical reactions take place on a part of microswimmers and they, thus, propel autonomously. Under magnetic field, microwsimmers can be driven and steered wirelessly. These microswimmers are demonstrated to have precise velocity and direction control.

The aforementioned microrotors and microswimmers are encouraging and provide innovative approaches for generating rotary motion in small scale. However, further improvements in fabrication[15,23,36,37] and higher performance are necessary to increase the practicality and applicability of these microstructures.[29,30]

1.3 Objectives

In order to bring solution to these problems, we combined the UV polymerization and acoustic for fabrication and actuation of microrotors and microswimmers. Simple fabrication and easy tunable actuation have the potential to significantly enhance the efficiency and performance of these micromotors and microswimmers. Since they are small enough, they have the potential for future applications in the field of biomedical engineering, biochemistry and biology in micro- and nanoscale.

Continuous or stop-flow UV polymerization techniques can yield complex microstructures for microfluidics in a simple fabrication.[28–30,71–73] However, easy actuation and high rotation rate are still needed for microrotors, micropumps, and microgears. In the last decade, various microscale acoustofluidic technologies have demonstrated simple, low-cost, contactless, and versatile operations in lab-on-a-chip applications[3,74,75] such as micromotors, micropumps[76] and micromixers.[77–80]

Acoustic microswimmers use acoustic streaming generated by acoustic waves. This streaming produces a force to move the microstructures.[38] On the other hand, some people have combined both of abovementioned sources in a system in order to utilize advantages of each. Chemical and acoustic propulsion is combined to utilize hydrogen peroxide decomposition and ultrasound for axial direction and speed control.[51] Also, magnetic field and acoustic have been used to propel and steer the nanowire motors.[50] Among these methods, acoustic propulsion has the edge over others due to contactless, inexpensive, and easy-to-operate actuation with small-scaled devices. Furthermore, acoustic waves do not need toxic fuel and are not harmful on biological samples. Therefore, acoustic is an appropriate candidate to power microrotors and microswimmers in biological and non-biological samples.

Chapter 2

Literature Review

2.1 Actuation of microstructures

Remotely powered and autonomous microrotors play an important role in microelectromechanical systems (MEMS),[10–13] biomedical engineering,[14–19] and biochemical applications.[20,21] They are used in lab-on-a-chip applications for mixing[22,23] and pumping,[24,25] or for studying the rheological properties of microdroplets or microparticles.[26,27] In order to achieve these lab-on-chip applications, different approaches are needed since viscous forces are dominant over inertial forces at low Reynolds number, contrary to macroscale actuation in which inertial forces are dominant. Thus, different actuation and fabrication approaches have been developed.

Additionally, microswimmers have grabbed the attention of scientists due to their practical and potential applications in small size.[38–46] Microswimmers having contactless actuation are appropriate for many applications such as targeted drug delivery, particle separation, mixing, pumping, assembly, manipulation, microsurgery and chemical analysis by mimicking their biological counterparts such as bacteria. [23,47–55]

Mimicking the biological microswimmers is a reasonable method to design artificial microswimmers in order to take advantage of natural orientation of biology.[16,47,52,56–58] Depending on the medium where biological microswimmers live, the flagella have been evaluated both experimentally and numerically to be rotated helically, spirally and wave sinusoidally.[8,9,43,59–62] Their design which enables them to move in

biological medium at low Reynolds number in microscale has been inspiring researchers to create decent artificial microswimmers.[9] Biological self-propelled microswimmers such as Escherichia coli (E. coli), human sperm, Chromatium okenii, Spirillum volutans and scallop have mechanisms to swim at low Reynolds number.[16,44,51,56,60,63,64]

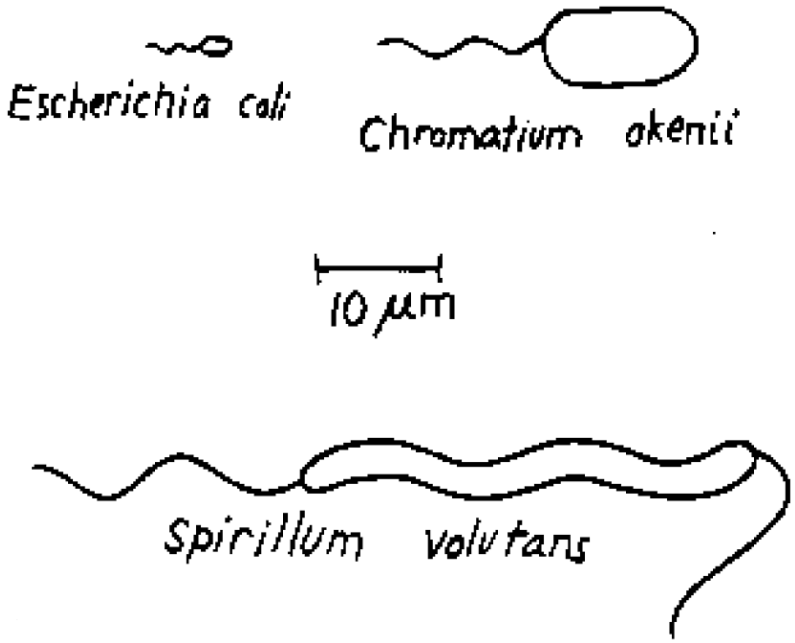

Figure 2-1 Schematic of real microorganisms swimming via waving their tail.[9]

Their tails, the flagella, propel and steer these microorganisms by oscillation in several form and these movements in turn enable the microorganisms to be motile to find their food, to reproduce and to move to safer place.

Microswimmers and microrotors can autonomously propel utilizing various energy types such as hydrodynamic force,[28] laser manipulation,[29,30] bacterial motion,[31–33] electrical, chemical, magnetic, acoustic and dual combination.[23,34,38,41,45,46,48,50,59,65–70]

2.1.1 Hydrodynamic force

Microrotors which are essential for many applications such as micropump and micromixer can be rotated by internal hydrodynamic force. Microrotors driven by hydrodynamic force are useful for torque transfer in micro scale through other microrotors. Moon *et al*. have demonstrated in situ fabrication and hydrodynamic driven of microrotors. They first fabricated microrotos inside a microchannel using a photocrosslinkable solution. They used UV light to polymerize the solution after patterning and focusing the UV light passing through a photomask and an objective lens. Therefore, only the intended shape of UV light reaches to the microchannel from the bottom layer.

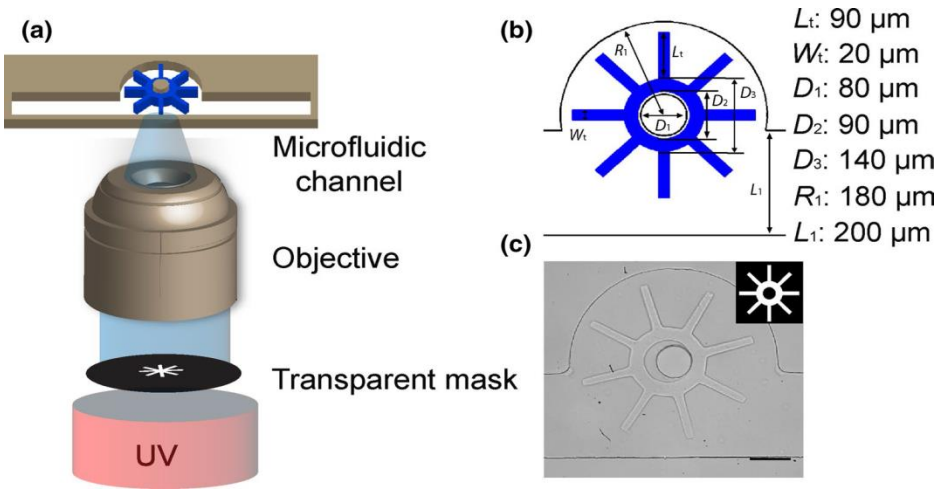

Figure 2-2 In situ fabrication of microrotor.[28]

After the fabrication, they wash away the photocurable solution inside the microchannel using PEGDA 250 and PEGDA700 which different viscosities, to get rid of rest of the photocrosslinkable solution. Since they fabricate the microrotors loosely around an existing pillar, the microrotors are able rotate freely. When injecting a flow through the

channel, the microrotors rotate. In detail, the flow creates an asymmetric flow pattern which results in a net rotation around the pillar.

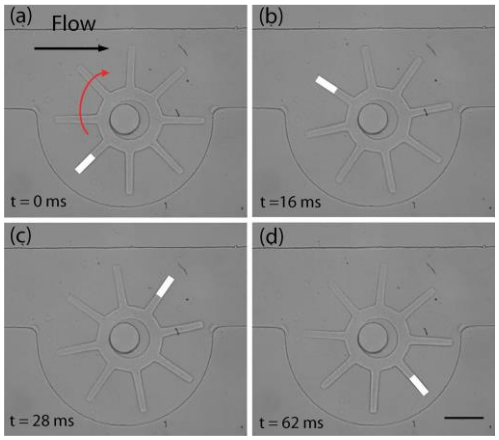

Figure 2-3 Rotation of microrotor by hydrodynamic force.[28]

After injecting the fluids (PEG250 and PEG700) at different flow rates, they analyzed the rotational speed of microrotors. The less viscous fluid, the more rotational they got. For example, their PEG250 fluid flow of 130 μl/min resulted in ~650 RPM.

2.1.2 Laser manipulation

Laser manipulation is another force of source to rotate the microrotors. Yue et al. demonstrated in situ fabrication and laser manipulation. Their fabrication method was UV polymerization which is discussed in the previous rotation method. Likewise, they applied patterned UV light from the bottom layer of microchannel which had photocrosslinkable solution inside.

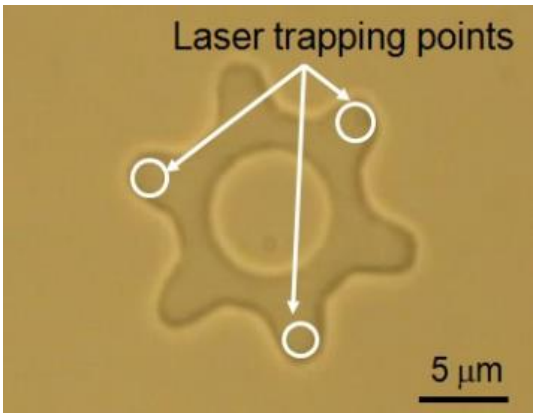

Figure 2-4 Laser trapping points on a microrotor.[29]

After washing away the photocrosslinkable solution inside the microchannel, they applied laser to rotate the microrotors. They used a galvanometer mirror to scan single laser and, therefore, form an arbitrary pattern via laser trapping. Eventually, multiple points were trapped at the end of tooth. These points were used to apply laser by trapping these tooth. Then, they used different solutions of viscosity. When the medium is less viscous (Ethanol), they reached higher rotational speed (30 RPM) when compared to the rotational speed (2.5 RPM) at high viscous solution of PEGDA. Their rotational speeds in both PEGDA and ethanol resulted in linear curve with laser power. Rotational speeds reached up to~5 RPM in PEGDA and~60 RPM at 2 watt laser power.

2.1.3 Bacterial force

Living organisms are capable of moving and sensing. As they are live organisms, they can be used to rotate the microrotors in a biological medium. Their self-propelling motions are

promising for biological and micromechanical applications. Leonardo et al. demonstrated self-propelled micromotors using bacteria as a drive source.

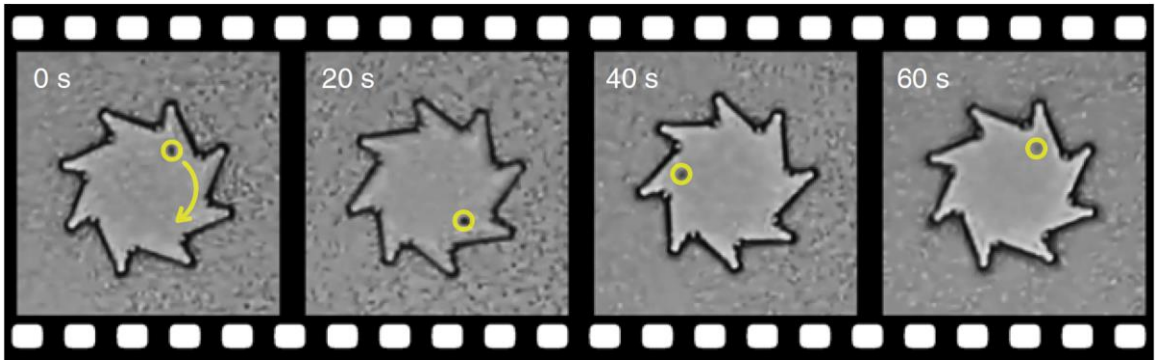

Figure 2-5 Microrotor rotation by bacteria.[32]

They used lithography as fabrication technique which requires clean room. Polymethyl methacrylate (PMMA) was the main material in this microrotor fabrication. Following the lithography, the whole wafer was waited in acetone and microrotors were unattached. Then, microrotors were centrifuged and resuspended in water.

As for microrotor rotation, asymmetrically designed microrotors were suspended in water with live bacteria. Because of asymmetry, bacterial motion was rectified and, therefore, microrotors rotated. Rotational speed of bacteria driven microrotors was around 1 RPM, which is not high when compared to other methods. However, this technique does not require external forces and is biocompatible, which makes it suitable micro manipulation method for biological applications.

2.1.4 Magnetic force

Magnetic force is commonly used technique to actuate mirorotors. Even though there are several fabrication methods such as lithography and UV polymerization, magnetic field, basically, is the source of actuation. Ryu et al. have demonstrated microfabrication of magnetic stir bar using lithography. Then they characterized a micropump utilizing magnetic field as driven force.

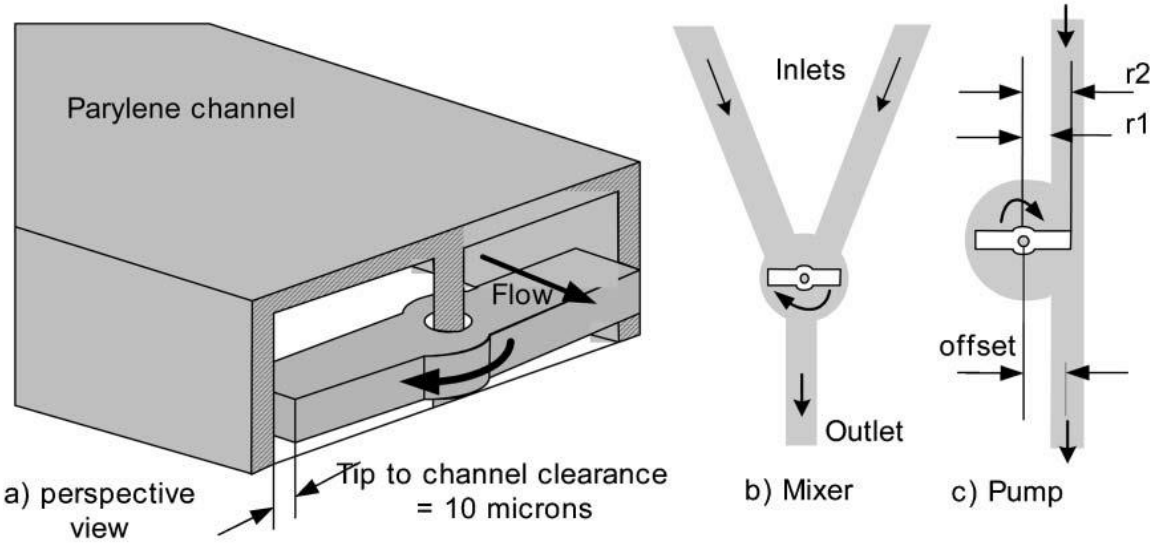

Figure 2-6 Lithographically fabricated micropump driven by magnetic force.[13]

Their rotational speed performance was good enough for biomedical applications. This performance was adjustable by tuning magnetic field. However, pumping performance (nl/min level) was not enough good due to physical constrains. Additionally, fabrication method requires long and expensive steps.

To simplify the magnetic micro actuation of microrotors, Chung et al. demonstrated in situ fabrication and magnetic actuation of microstructures. In their approach, they embedded magnetite (Fe_3O_4) which was able to be manipulated via

magnetic field, into photocrosslinkable solution inside microchannel. After applying UV light, the rest of photocrosslinkable solution was washed away. The microrotors were able to rotate freely and transport liquid thoroughly.

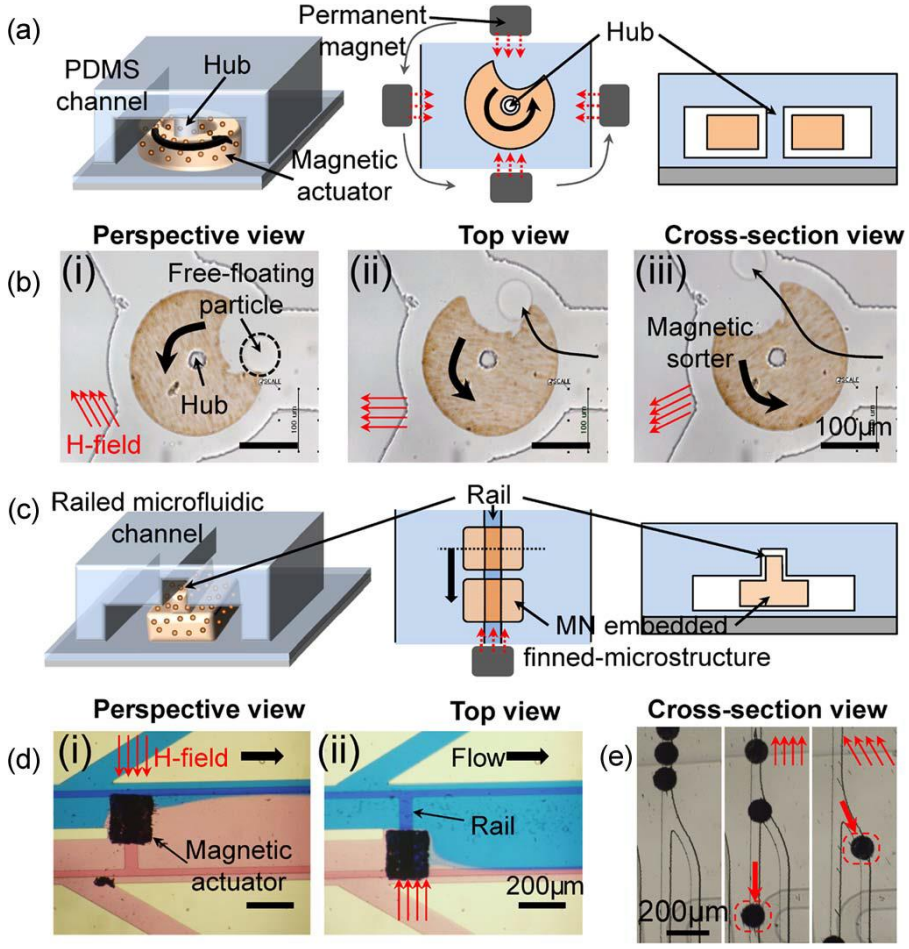

Figure 2-7 Magnetic actuation of in situ fabricated microrotors.[71]

Peyer et al. demonstrated magnetically actuated swimmers by mimicking the bacterial helical flagella propulsion. After the fabrication of microswimmers using clean room activities including lithography and direct laser writing. In order to actuate the microswimmers, they used orthogonal Helmotz coil pairs in their experiments. Helical

motion of these artificial microswimmers propelled them. By controlling the magnetic field, the direction and angular speed can be controlled using this method.

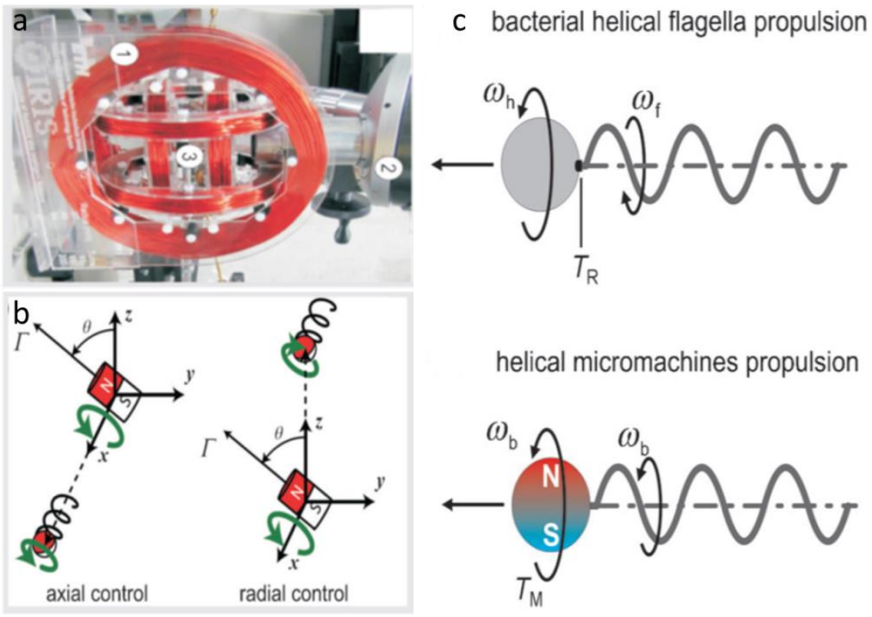

Figure 2-8 Magnetic actuation of bacterial mimicked microswimmers.[59]

2.1.5 Chemical propulsion

Chemically propelled microrotors under electric field is an effective locomotion method to actuate. It requires unique design and fabrication. Loget et al. demonstrated microobjects driven by electric field. Their fabricated microrotors using a conductive polycarbonate sheet. One face of the ends of 4-arm sheet were covered with conductive part. This part was able to take part in chemical reaction under electric field. Then, the sheet was placed between anode and cathode. For the actuation, electric field of 0.5 kVm^{-1} in 50 mMHCl and 100mMHO medium was applied. The chemical reaction in the conductive part produced Hydrogen bubbles which forced the microrotor to rotate. The rotational

performance was as low as ~ 1 RPM. However, this method can be used in biochemical applications in micro scale.

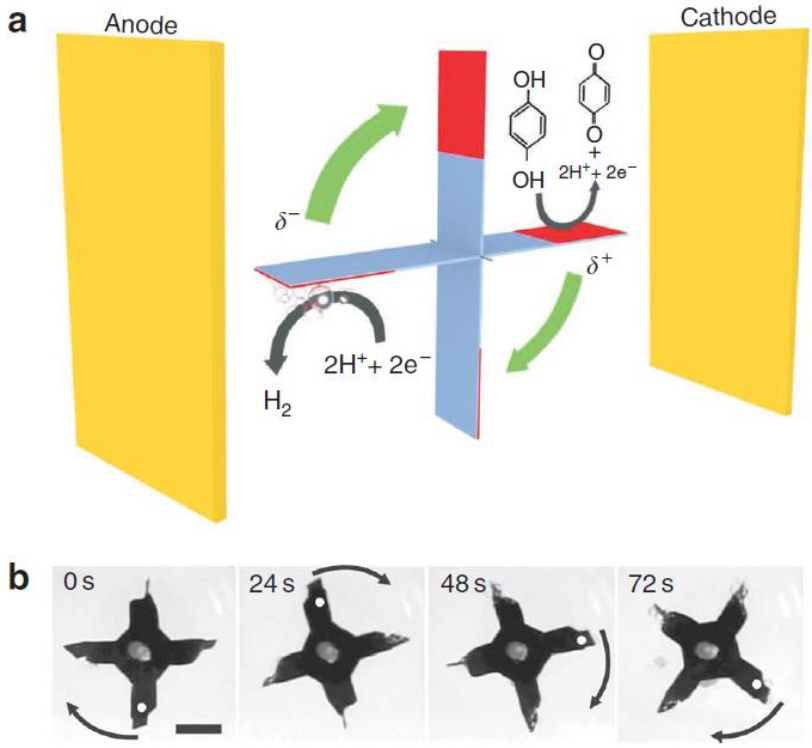

Figure 2-9 Rotation mechanism of chemical microrotors.[34]

Another chemical microswimmers are Janus colloids. Simmchen et al illustrated that these chemically driven microswimmers were fabricated comprising of active and non-active part by coating the one side with platinum and other side with hydrogen peroxide. Hydrogen peroxide was the active part of Janus microparticle. The active side on the microparticle decomposed in water medium and, in turn, Janus microparticles moved. Then, they used surface effect to guide them. When the Janus particle placed next to wall of microchannel, they followed the trajectories along the edge of the wall. Their Janus microparticles were able to move and follow trajectories without external forces,

which is an advantage for applications that require autonomous control. Major drawback of these microparticles is that they have limited fuel. This limitation does not allow them to be used for long applications.

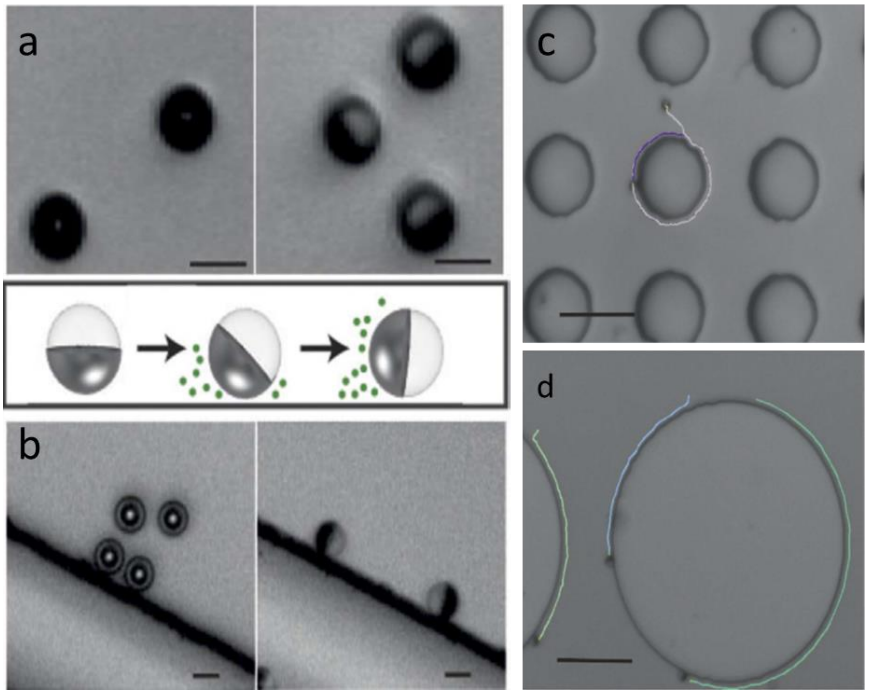

Figure 2-10 Propelling and guidance mechanism of chemical microparticles.[46]

2.1.6 Acoustic waves

Acoustic waves are used to power microstructures in form of surface acoustic waves (SAW) and bulk acoustic waves (BAW). Shilton et al. reported a high performance microrotor driven by SAW. They first fabricated gold interdigital transducers (IDTs) onto the lithium niobate ($LiNbO_3$) substrate via lithography in clean room. Then they placed a disc rotor which could rotate freely in the middle of lithium niobate substrate. In order to

make the disc rotor freer, the cover middle of lithium niobate substrate with Teflon material.

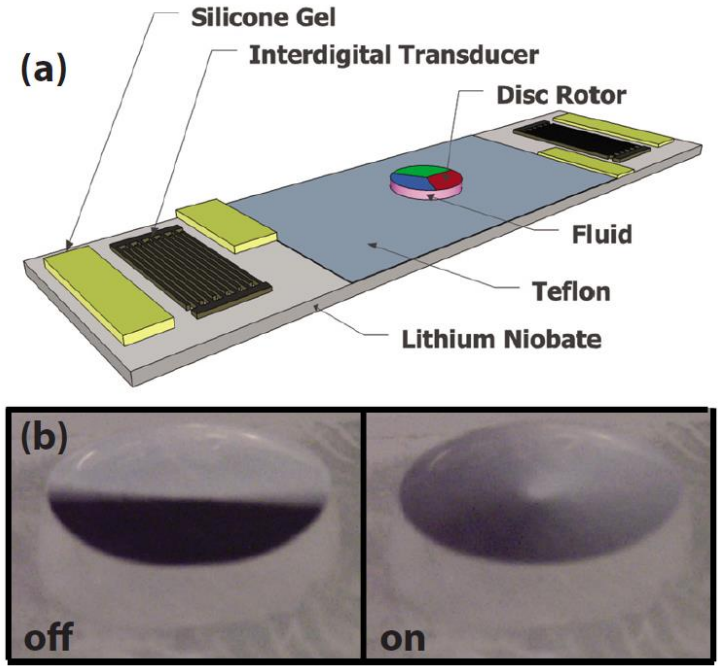

Figure 2-11 Surface acoustic wave (SAW) rotation of a disc rotor.[37]

In front of half of the IDTs, they placed silicone gel which were located opposed in the corner of IDTs to dump the half of the SAW and break the symmetry. This asymmetry allowed SAW to rotate the disc rotor. Though their fabrication is time consuming and expensive, microrotor had high performance of over 2000 RPM.

BAW is also useful acoustic wave due to its easy operation and cheapness. Ahmed et al. illustrated microswimmers which were powered by a transducer. They in situ fabricated these swimmers via UV light. After this single step fabrication, they trapped bubbles inside holes located in different parts of the microswimmers depending on the

actuation purpose. In order to actuate the microswimmers, a simple piezoelectric (PZT) transducer was bonded next to microfluidic channel. Upon application of the transducer, the bubbles oscillated and, therefore, generated a net force which moved the microswimmers either directionally of rotationally.

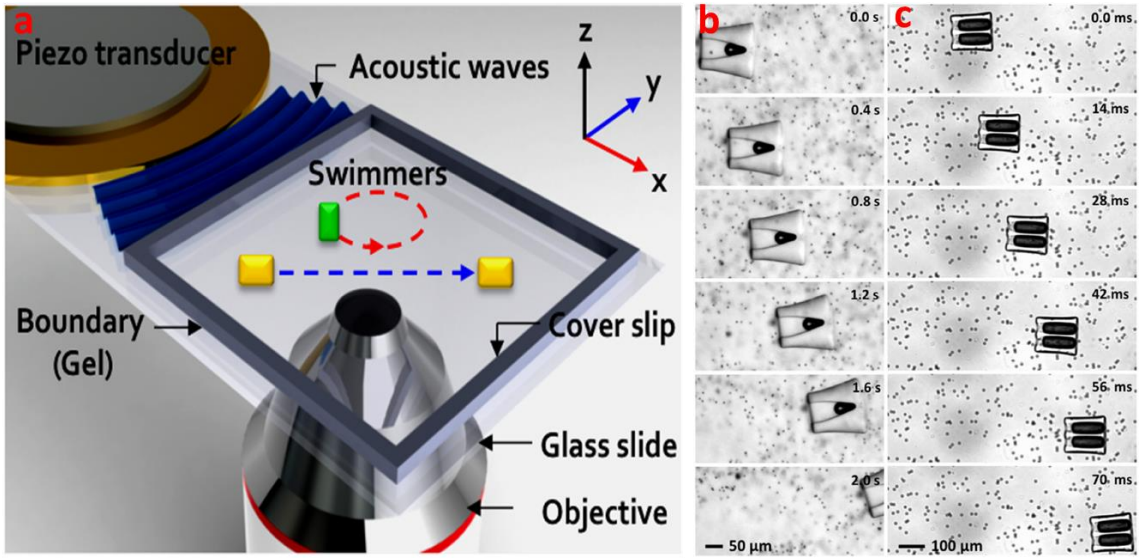

Figure 2-12 Bulk acoustic waves actuation of in situ fabricated microswimmers.[38]

Their technique compiles easy fabrication and actuation using low power (a few volts). Yet, bubble trapping is not as easy as actuation. Furthermore, trapped bubbles can get bigger in time of experiments. Therefore, these microswimmers are not suitable for long term need.

2.1.7 Dual combination of actuation methods

Combination of two actuation methods for further application has been attractive to people. For example, Wang et al. illustrated that bimetallic gold-ruthenium microrods motion in

water. This bimetallic microrods followed a trajectory when only chemical propulsion by catalytic decomposition of hydrogen peroxide was applied. Then, acoustic was turned on. The microrods changed its trajectory and followed another one. This is very promising combination to stir the microrods.

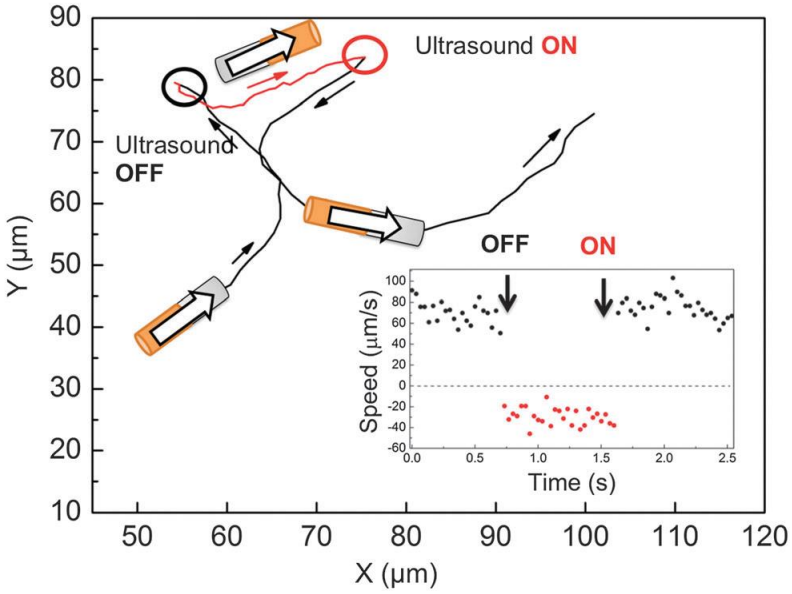

Figure 2-13 Stirring a chemical microrod under acoustic field.[65]

Stanton et al. demonstrated that magnetic field and chemical propulsion can be mutually used to propel and control the microswimmers in order to transport biological microorganisms such as Escherichia coli (E.coli). Upon the fabrication of magnetic microswimmers with Janus particles, E.coli was adhered to them. The trajectories without magnetic field was back and forth in time. When the magnetic field was on, Janus particles followed another trajectory which was quite straight.

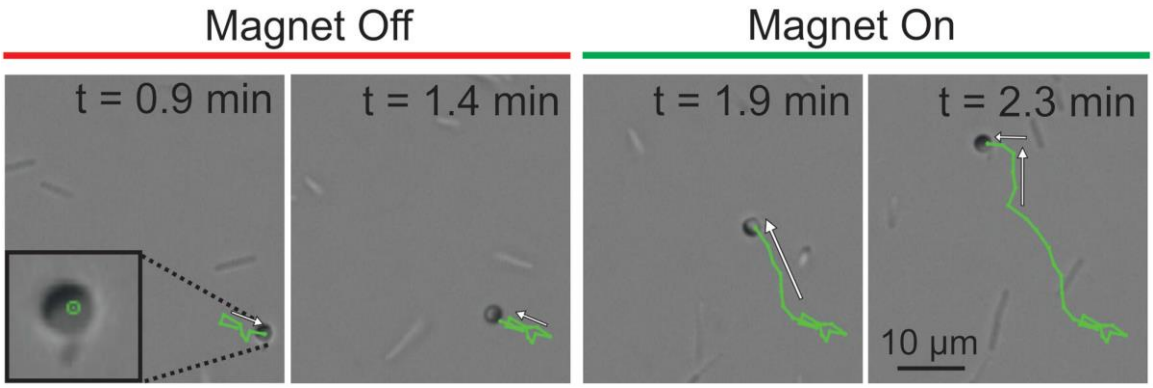

Figure 2-14 Magnetic control of Janus particles attached with E.coli.[51]

Ahmed et al. illustrated that acoustic propulsion and magnetic field are an effective way to control the nanowires. After they fabricated the nanowires which are sensitive to acoustic and magnetic field, they first applied only acoustic. Then, they tracked the nanowires under both acoustic and magnetic field. This mutual technique can be used in biological applications such as microsurgery and drug delivery.

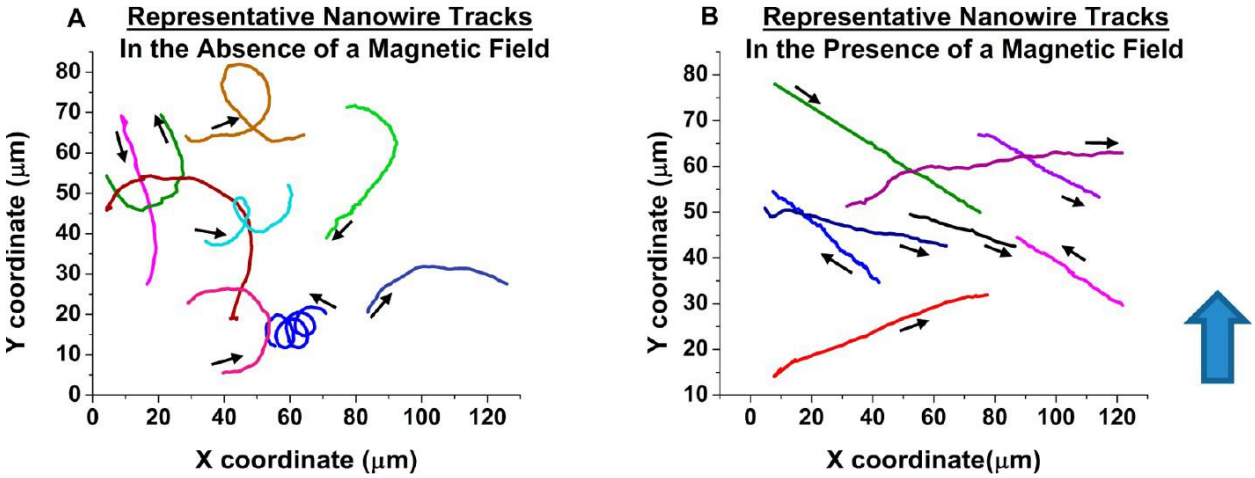

Figure 2-15 Tracks of acoustically propelled nanowires with and without magnetic actuation.[55]

Chapter 3

Methodology

3.1 Device fabrication, experimental set up and acoustic actuation

First, a single-layer PDMS microchannel (containing micropillars that act as axles) was fabricated using soft lithography and replica molding. We pretreated a silicon wafer with hexamethyldisilazane (HMDS), patterned in photoresist (Megaposit SPR955, Microchem, USA), and etched using deep reactive ion etching (DRIE). To reduce the surface energy of the silicon wafer and ease the peeling of the PDMS channel, we coated the silicon master with chlorotrimethylsilane (75-77-4, Alfa Aesar, USA). The PDMS microchannel was fabricated by curing a 10:1 mixture of PDMS resin and curing agent (Sylgard 184, Dow-Corning, USA) at 65°C for 2 h. Then we peeled off the PDMS layer from the mold and used a reusable biopsy punch (Harris Uni-Core 0.75 mm) to punch holes for inlet and outlet. The PDMS channel is 100 μm deep and 2 mm wide in the region where UV polymerization and acoustic actuation occur. Later, we coated a glass slide (48404-454, VWR, USA) with PDMS using a spin coater (WS-650MZ-23NPP/Lite, Laurell Technologies, Czech Republic) at 1000 RPM for 1 minute, and baked at 65°C for 30 min. The PDMS microchannel was bonded onto the PDMS coated glass slide and the whole device was baked at 65°C for 2 h.

For in situ microstructure fabrication, a mercury lamp (Intense Light C-HGFI, Nikon, Japan) provided the white light source. A computer controlled mechanical shutter (LB-SC, Sutter Instrument Company, CA, USA) controlled UV exposure time,

in our case 50 ms. An inverted microscope (Nikon TE-2000U) equipped with a 10x objective lens (Plan Fluor 10x/0.3 DIC L/N1, infinity/0.17 WD 16.0, Nikon, Japan) and a filter cube (11000v3: UV, Chroma) was used for in situ fabrication of microstructures into these channels.

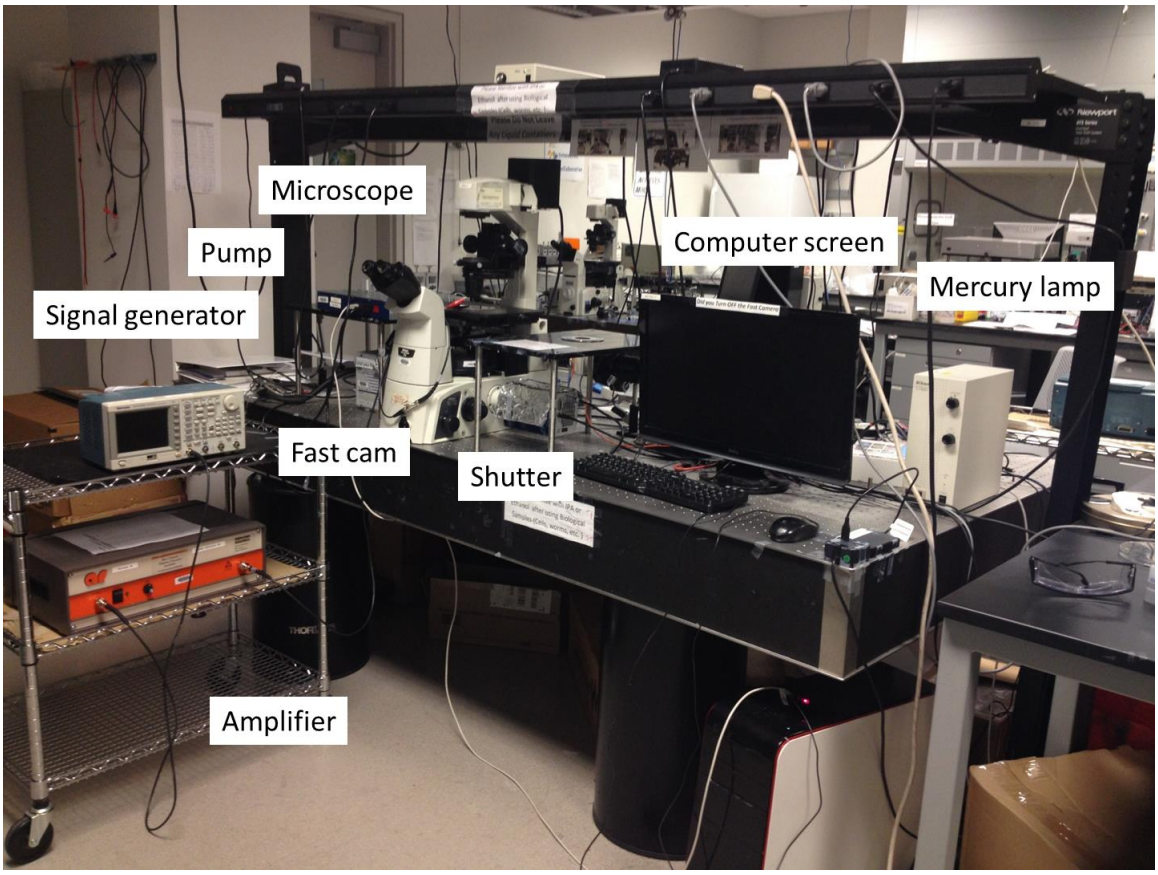

Figure 3-1 Experimental set up to fabricate and actuate microstructures.

The UV light intensity exiting the 10x objective lens was measured as ~ 80 μW/cm2, which was fixed in our experiments, using a power meter (FieldMaxII-TO Laser Power/Energy Meter, Coherent Inc., USA). The UV light, then, entered the microchannel and polymerized the intended microstructures. A transparent photomask containing the rotor design was placed into the field-stop slot of the microscope. A

solution consisting of 40% (v/v) polyethylene glycol (PEG) diacrylate with a molecular weight of 700 (PEG700, Sigma-Aldrich, MO, USA), 25% (v/v) PEG with a molecular weight of 258 (PEG 258, Sigma-Aldrich, MO, USA), 15% (v/v) photo-initiator 2-Hydroxy-2-methyl-1-phenyl-propan-1-one (Darocur 1173, from Ciba), 15% (v/v) TE buffer (100 TE, from OmniPur), and 5% (w/v) Rhodamine 6G, was injected into the PDMS microchannel through the inlet by a 1 ml syringe (McKesson, CA, USA).

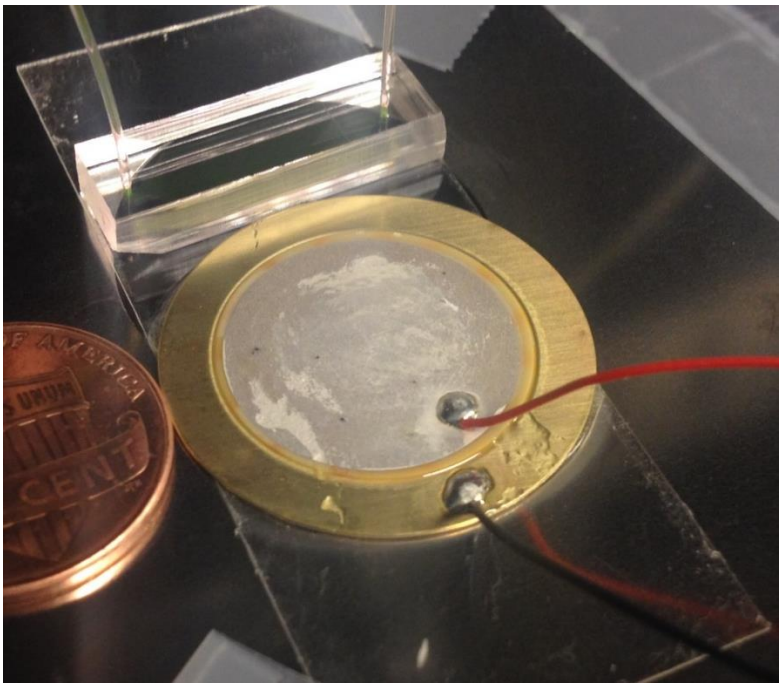

Figure 3-2 The whole microdevice

After the injection we waited 5 minutes to ensure that solution flow inside the channel came to a full stop. The axle pillar and the rotor pattern in the photomask were then aligned concentrically for microrotor fabrication. Note that microswimmers do not need this alignment. Upon UV exposure and polymerization, the microrotors and microswimmers form in situ axle inside the microchannel. After fabrication, we washed

away the un-polymerized solution in the microchannel with an ethanol solution, observing no significant shape deformation of the microstructures. Figure 3-3(b) and Figure 3-3(d) provide perspective schematic views of a microrotor and microswimmer, respectively. The UV polymerized microstructures are able to rotate and move freely in an ethanol medium without adhering to the substrate or axle. PDMS is an oxygen-permeable material that forms a thin oxygen inhibition layer near the PDMS channel boundaries both at the bottom and the top, and constrains the PEG from UV-polymerizing near PDMS walls.[71,81–85]

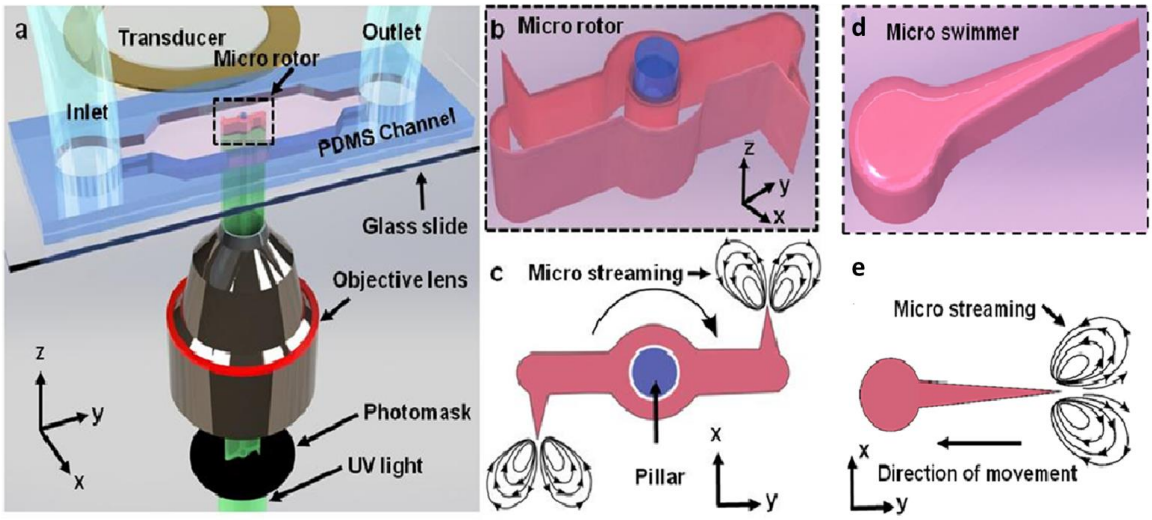

Figure 3-3 (a) Schematic of fabrication and actuation set up (not to scale). A mask and an objective lens are used for patterning and focusing UV light, respectively. (b) Schematic of microrotor which is fabricated around existed PDMS pillar (diameter: 90 μm) and able to rotate freely. The depth of the fabricated microrotors is ~ 96 μm which is slightly smaller than the channel height due to the oxygen inhibition layers (c) Schematic of acoustically actuated two-arm microrotor. The end-to-end distance and the inner diameter of the microrotor are 550 μm and 100 μm, respectively. (d) Schematic of acoustically actuated directional microswimmer. The length of the microswimers is ~ 180 μm while the height is ~ 46 μm. When the acoustic field is present, sharp-edge structures oscillate and generate acoustic streaming and, therefore, (e) a microswimmer move directionally.

For actuation, a piezoelectric transducer (81-7BB-27-4L0, Murata Electronics, Japan) was bonded next to the PDMS device (see Fig. 1a) on the same glass slide using a thin layer of epoxy (G14250, MA, USA). Activation of the piezoelectric transducer was controlled by sine-wave signals from a function generator (AFG3011, Tektronix, USA) amplified by an RF amplifier (25A250A, Amplifier Research, USA).

Chapter 4

Results

4.1 Acoustofluidic actuation of in situ fabricated microrotors

In this chapter, in situ fabrication and acoustic actuation of microrotors are demonstrated. Rotational speeds and microstreaming around the sharp-edge structure was characterized. We fabricated microrotors without sharp-edge structures and with sharp-edge structures on the same or opposite sides of microrotors to demonstrate the proof of the concept for rotational actuation, as shown in Fig. 2.

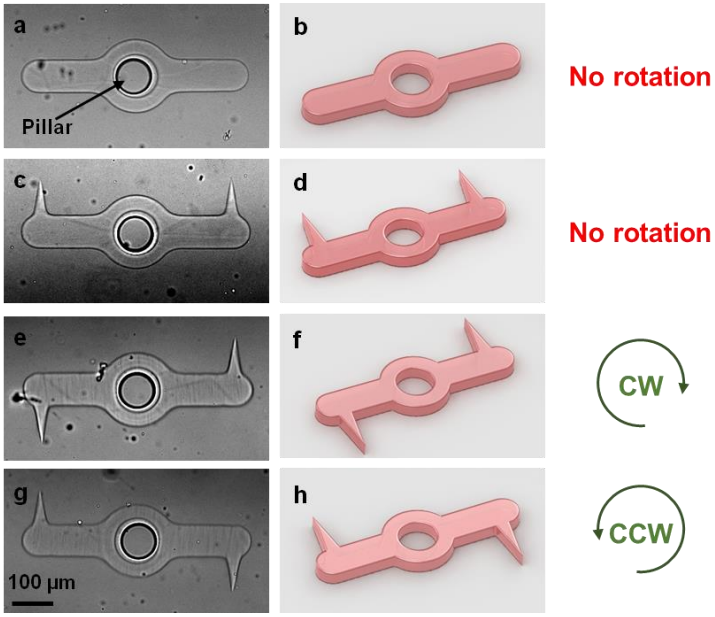

Figure 4-1 Image and schematic of proof of concept, which illustrates the effect of sharp-edge structures on rotation. (a), (b) image and schematic of 2-arm rotor without sharp-edge structure which is not supposed to rotate. (c), (d) Relative placement of sharp-edge structures results in cancelling torques. No rotation is expected. (e), (f) The microrotor rotates clockwise because of the position of sharp-edge structures, which creates a net torque from acoustic streaming. (g), (h) The microrotor rotates counter-clockwise due to the position of the sharp-edge structures.

The microstructure without sharp-edge structures (Figure 4-1a,b) does not generate significant acoustic streaming and thus did not rotate under acoustic drive. When the sharp-edge structures are on the same side of the two-arm structure (Figure 4-1c,d), there was no net rotation because the acoustic streaming cannot impose a net torque on this mirror-symmetric structure. On the other hand, when the sharp-edge structures are situated on opposite sides of the two-arm rotor, acoustic streaming produces a net torque on the microrotor and we obtained clockwise (CW) and counter-clockwise (CCW) rotation, shown in Figure 4-1e–h. We can fabricate CW or CCW rotating microrotors with one photomask, simply by flipping the photomask in the field stop.

The angular speed of the microrotors was characterized as a function of the driving frequency. The maximum angular speed occurred near 4.3±0.3 kHz which is slightly lower than the nominal resonant frequency of the transducer (4.6 kHz). However, as shown in Figure 4-2a, bonding the transducer to the glass slide lowers its resonant frequency to ~ 4.4 kHz which agrees reasonable well with the frequency of highest angular speed.

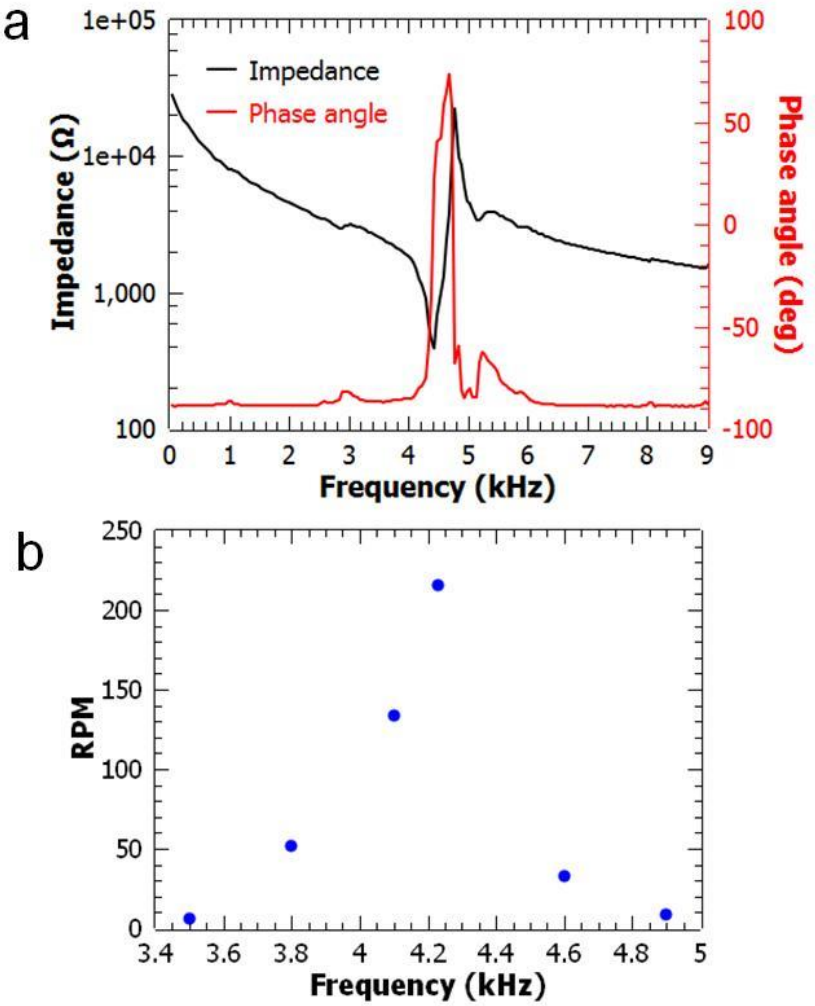

Figure 4-2 Resonance frequency analysis of a bonded transducer. (a) Impedance and phase angle measurements of the bonded transducer yield a resonant frequency of 4.41 kHz. (b) Dependence of the rotational rate of a one-arm microrotor to the frequency shows a maximum performance at around 4.25 kHz.

Next, we investigated the effect of the number of arms on rotational performance, to determine whether the individual arms contribute additively, or if interactions between the streaming fields of nearby arms may enhance or degrade the overall performance of the device. All arms have the same size, with one sharp-edge structure on each trailing edge, as shown in Figure 4-3a–f. Figure 4-3g shows the performance of microrotors with from 1

to 6 arms. Due to geometrical constraints, we could not increase the number of arms beyond 6. The peak-to-peak voltage (VPP) in Figure 4-3g was fixed at 160 VPP (the maximum voltage applied in this study). The angular velocity is nearly linear in the number of arms, varying from ~ 200 RPM for one arm to ~ 1200 RPM for six arms.

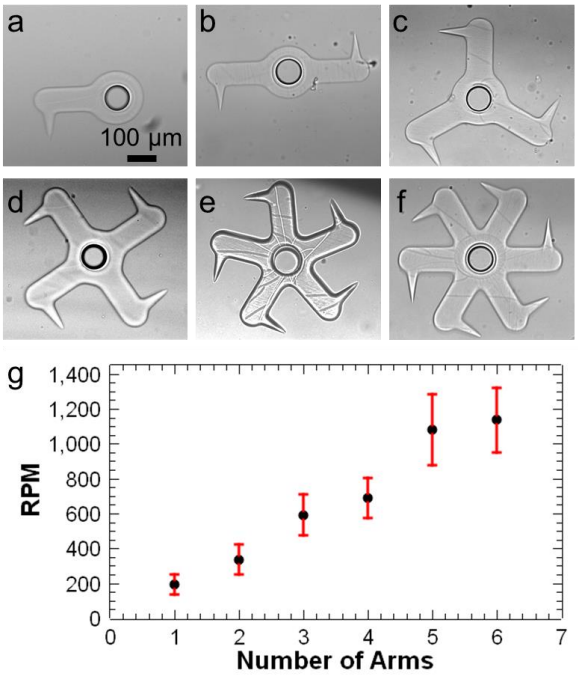

Figure 4-3 Microrotors with different numbers of arms. (a)-(f) images of 1-arm to 6-arm microrotors fabricated around existed pillar. (g) Angular speed vs. number of arms. With the incremental number of arms around the pillar, angular speed increases because the more sharp-edge structures, the more acoustic streaming and force that can be generated. Error bars represent standard deviation of five or more repeated experiments.

If the propulsive contributions of individual arms are largely independent of each other, then this result suggests that the drag force on the rotor is largely independent of the number of arms, i.e., arises predominately from the axle region. The similar sizes of the gaps between the axle and rotor and between the rotor surfaces and the top and bottom of the microchannel then suggest that the forces impeding rotation do not arise exclusively

from viscous drag at these interfaces (otherwise, the drag on the arms would dominate). This conclusion is consistent with the threshold voltage necessary to initiate sustained motion being somewhat lower for the rotors with more arms. When the acoustic field was turned off, a 4-arm microrotor came to a full stop after 1.8 milliseconds and ~ 2 degrees of further rotation. This rapid slowdown is promising for applications that require discrete step-wise rotation.

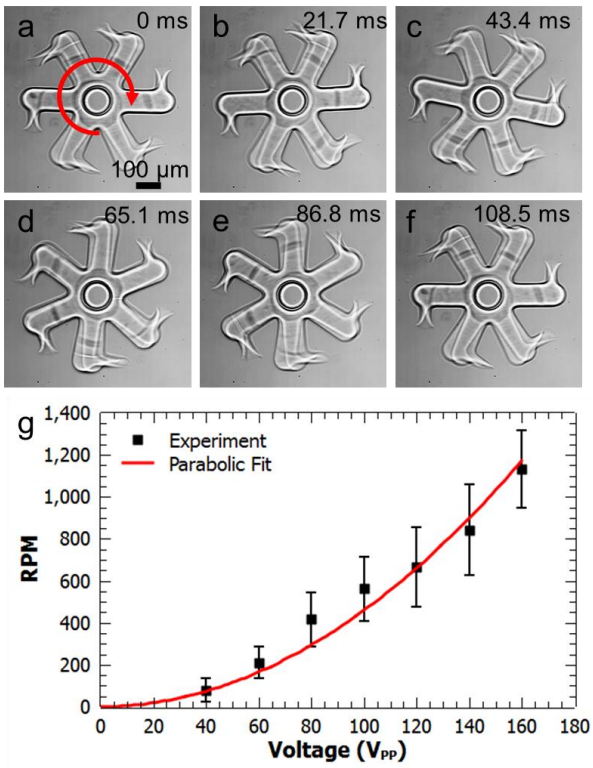

Figure 4-4 (a)-(f) Image series for an acoustically actuated 6-arm microrotor, showing a full rotation across 6 frames. (g) RPM versus peak-to-peak voltage for a 6-arm microrotor, showing an increase of the angular speed with the applied voltage amplitude, above a small offset voltage (20–30V) necessary to initiate motion. Error bars represent standard deviation of five or more repeated experiments. The coefficient of parabolic fit is 0.0458.

The acoustic streaming is controlled by the amplitude of the transducer voltage, which provides straightforward tunability of the rotation rate. Figure 4-4 shows the angular

speed of an acoustically actuated 6-arm microrotor as a function of the applied peak-to-peak voltage from 40 VPP to 160 VPP. A parabolic relation here is consistent with the second-order nature of acoustic streaming, if one assumes that the overall velocity of the rotor structure scales linearly with the rate of momentum transfer from acoustic streaming and that the amplitude of sharp-edge structure motion is linearly proportional to the drive voltage. However, considering that the overall rotor motion is not in the limit of small Reynolds number (see below) and there is a modest threshold voltage needed to obtain sustained motion, one much also consider the possibility that the relation is more complex. Below 40 VPP rotation was less than 6 RPM. Figure 4-4a-f show one full clockwise rotation of the 6-arm microrotor at 100 VPP divided into 6 frames, one rotation being completed in 108.5 milliseconds. As shown in Figure 4-4g, the angular speed of an acoustically actuated 6-arm microrotor monotonically increases from ~ 550 RPM at 100 VPP to ~ 1200 RPM at 160 VPP.

As an application of the acoustically actuated microrotors, we have demonstrated mixing of two fluids using a 6-arm microrotor actuated at 160 VPP. In this simple example, we injected ethanol solution with suspended fluorescent beads and pure ethanol into the microchannel at a total flow rate of 10 μl/min. Upon the application of acoustic field, the microrotor mixed the two fluids in under 30 milliseconds.

A linear system subjected to monochromatic sinusoidal actuation oscillates at the frequency of the driving force. Our microrotor systems are driven by an acoustic signal with a frequency of several kHz. The immediately observable responses are oscillation of the sharp-edge structures at the ends of the arms at the drive frequency (see Figure 4-5) and steady rotation of the entire microrotor, which is really a zero-frequency motion

because it is not oscillatory. This zero-frequency motion must be due to nonlinearities in the dynamics, and is very likely due to so-called acoustic streaming.[86,87] Acoustic streaming originates from dissipation in the fluid, either in the boundary layer (resulting in boundary-layer driven streaming) or in the bulk fluid. The relative contribution of these mechanisms to the mean flow generation depends on the size of the device. Since our device is much smaller than the inverse of the spatial damping rate, we expect weak interior dissipations in our device.[88] Thus, we believe the boundary-driven streaming to be the dominant mechanism in our devices. However, by retaining the bulk viscosity terms in our numerical formulation, we have considered both mechanisms of acoustic streaming in our numerical results. The acoustic streaming patterns are schematically depicted in Fig. 1c and are experimentally visualized in Fig. 5a with the aid of 1 μm diameter fluorescent tracer particles.

To numerically investigate the acoustic streaming, we followed the previously reported perturbation approach[86] where we split the flow variables into first- and second-order components. Upon substitution into the balance laws, this results in two separate sets of first- and second-order equations which are then solved successively to predict the response of the fluid. Figure 4-5b shows numerically computed particle trajectories which appear to be in good qualitative agreement with the observed flow patterns visualized in Figure 4-5a. The non-symmetric nature of the streaming patterns around the tip of sharp-edge structure can be attributed to the inherent asymmetry in the geometry of the arm of the microrotor as well as a slight tilt of the sharp-edge structure that may result from the fabrication. Significant nonlinear effects indicate that the local Reynolds number should not be small. Reynolds number is a characteristic

speed times a characteristic length divided by the fluid kinematic viscosity (UL/ν). It is precisely defined, but not often unique since different parts of a system (*e.g.*, sharp-edge structure, arm) may have different sizes and may move with different characteristic velocities.

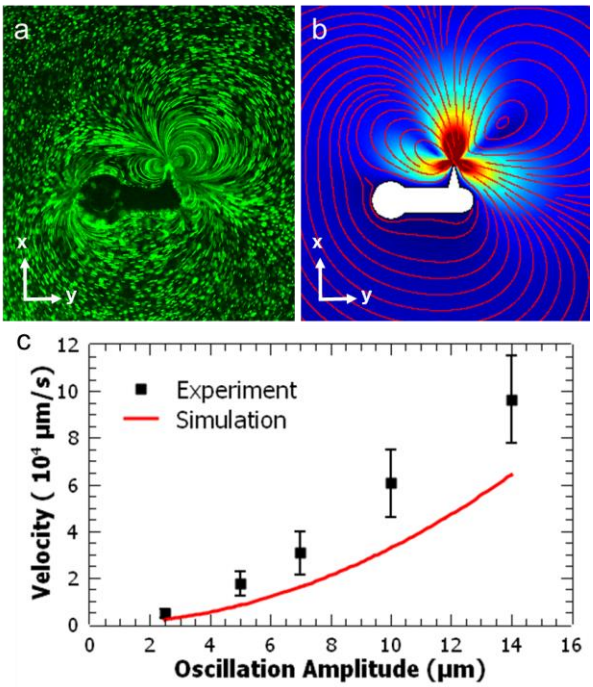

Figure 4-5 Acoustic streaming patterns around oscillating of a one-arm structure. (a) Fluorescent microscopy images of 1 µm polystyrene beads are stacked to visualize the vortices. (b) Streaming flows are numerically produced using perturbation approach. (c) Experimental and numerical analysis of streaming velocities ~ 40 µm away from the tip of the along the x axis. The coefficient of the numerical curve is 0.0326 $(\mu m\ s)^{-1}$.

At 160 V_{PP}, oscillation of the 100 µm long sharp-edge structure is 100 µm peak-to-peak, giving an average tip speed of $U \approx 4 \times 10^5$ µm/s. With L ≈ 100 µm, the length of sharp-edge structure, and $\nu = 1.5 \times 10^6$ $(\mu m)^2/s$, the kinematic viscosity of ethanol, this motion corresponds to a Reynolds number of approximately 26. While this is the Reynolds number relevant to the streaming, it is interesting to note that the overall

rotational motion is also not in the low-Reynolds number regime. At 1000 RPM, the end of the rotor that is 275 μm from the axle center has a speed of U ≈ 3 x 104 μm/s. With L ≈ 275 μm, this gives a Reynolds number of about 5.5. The Reynolds number associated with the small gaps between the rotor and the upper and lower surfaces of the channel is proportionately smaller.

To experimentally characterize the streaming speeds for different values of tip displacement, we analyzed the motion of 1 μm diameter polystyrene beads. Figure 4-5c shows a quantitative comparison between the experimentally measured and numerically predicted streaming speeds with a coefficient of 0.0326 $(\mu m\ s)^{-1}$ at a position 40 μm away from the tip of sharp-edge structure along the x-axis for different values of the tip displacement. The plot shows semi-quantitative agreement between the experiments and numerical simulations. The differences may be due to the structural imperfections or lack of precise knowledge of the vibrating profile of the sharp-edge structure. Nonetheless, the numerical model can predict the trends concerning with the effects of various geometrical and operational parameters on the acoustic streaming flow, and thus is useful for design and optimization. Both in experimental and numerical results, the streaming speeds scale quadratically with the vibrational amplitude, consistent with the streaming flow being second-order in the velocity (or equivalently, the displacement amplitude).[86,87]

4.2 Acoustic Actuation of Flagellated Microswimmers

In this chapter, acoustic actuation of biologically mimicked microswimmers is experimentally developed. First, microswimmers are in situ fabricated by using UV light in a microchannel fulfilled with a photocrosslinkable solution. When acoustic waves are applied, the flagella of microswimmers oscillate, which, in turn, moved them either rotationally or directionally depending on the design.

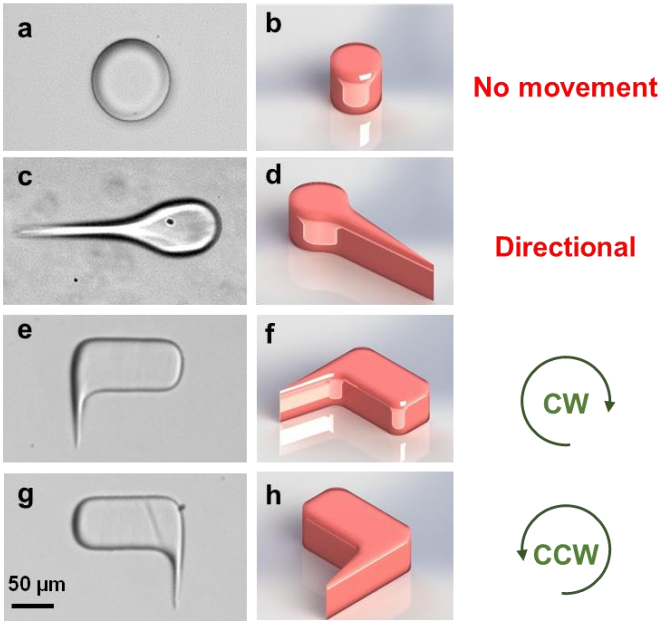

Figure 4-6 Design of different microswimmers (a) and (b) image and schematic of a microstructure which is not able to rotate. (c) and (d) microswimmer moves directionally due to acoustic streaming. (e) and (f) the oscillation of flagella creates clockwise rotation due to unsymmetrical design. (g) and (h) microswimmer rotates counter-clockwise.

Figure 4-6 shows the proof of concept, which microswimers with flagellated tail can swim under acoustic field. We, first, fabricated microswimmers without flagella. (See Figure 4-6a, b). When applying acoustic, there was not significant acoustic streaming. Thus, this microstructure did not swim under acoustic field.. In order to get directional

movement, we fabricated a symmetrical microswimmer having a head and a tail mimicking flagella as bacteria. The head and flagella of microswimmer were expected to oscillate at different amplitudes due to different size of each part even though the whole microswimmer was under the same acoustic drive. Therefore, the microswimmer swam directionally on the axis from tail to head, shown in Figure 4-6c, d. When breaking the symmetry in the microswimmer design, we obtained rotational microswimmers (see Figure 4-6e-h). A clockwise rotation was observed when the flagellum was situated at the left edge of microswimmer. On the other hand, the flagellum at the right edge generated counter clockwise rotation. The microswimmers rotated oppositely at the same time under the same acoustic drive.

The maximum directional and rotational performance of the microswimmers were obtained under the resonance frequency of the transducer, which is 4.6±0.5 kHz. Below and above this frequency, we did not get satisfactory performance both directionally and rotationally.

Next, we investigated that different microswimmers could swim under the same acoustic drive at the same time (Figure 4-7). In the Figure 4-7a, two different microswimmers are at a standstill under no acoustic drive. Both microswimmers have the same geometry and size with a flagellum to propel them. By applying acoustic field of 100 pick-to-pick voltage (V_{PP}), both microswimmers started to swim through each other at a similar velocity of ~ 600 μm/s (Figure 4-7b). Note that their trajectories are quite straight on the axes from flagellum to head. The microswimmers touched each other on the slightly left of the middle (Figure 4-7e). They still continued their directional movement after being unstuck.

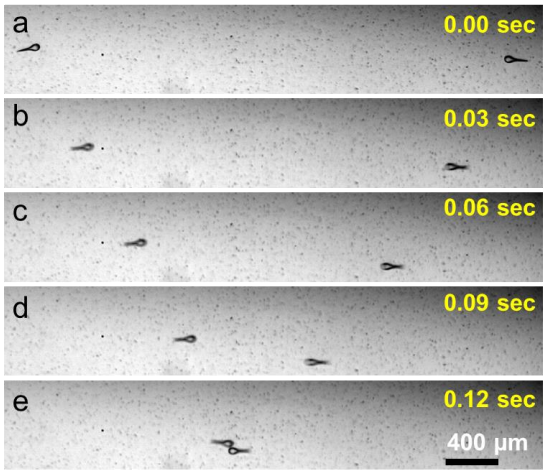

Figure 4-7 Opposing movement of microswimmers under the same conditions. (a) Both microswimmers do not have oscillations in their flagella and, therefore, no movement happens due to lack of acoustic actuation. (b), (c), (d) and (e) Microswimmers swim opposingly each other at 160 V_{PP}. They follow the same pathway and meet.

Acoustic streaming increases as a function of pick-to-pick voltage as the oscillation of a flagellum increases. Therefore, the more oscillation of flagellum of the microswimmer the more force to propel and rotate the flagellated swimmers we could get. Figure 4-8 illustrates the function of terminal velocity of flagellated directional microswimmers under different values of V_{PP} from 40 V_{PP} to 160 V_{PP}. Figure 4-8a-d shows the motion of a flagellated directional microswimmer when applied 100 V_{PP} by indicating each frame of 0.4 seconds. The flagellated microswimmer directionally swam and equally proceeded the same distance as a result of equal amplitude of flagellum oscillation in each interval, as shown Figure 4-8a-d. The terminal velocity of flagellated directional microswimmer is ~ 200 µm/s at 40 V_{PP} while it increases steadily over ~ 1200 µm/s at 160 V_{PP}. Below 40 V_{PP}, the velocity is quite close to zero. 160 V_{PP} was the maximum voltage applied in this study.

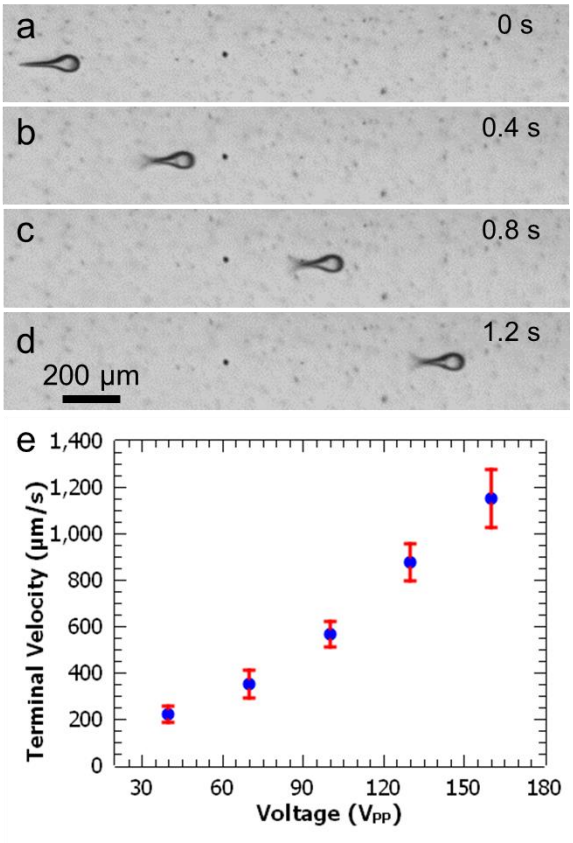

Figure 4-8 Characterization of microswimmers' directional movement. (a) Microswimmer has no acoustic oscillation. Thus, no movement is performed. (b) Actuating the PZT transducer, microswimmer's flagella oscillates and move directionally at 160 V_{PP}. (c) and (d) microswimmer can swim equal distance under the same voltage (160 V_{PP}) in a given time (0.4 s). (e) Terminal velocity of microswimmers in response to different values of voltage. Microswimmer can swim ~ 220 µm/s at 40 V_{PP} with an increase up to ~ 1200 µm/s at 160 V_{PP}.

Oscillation of the flagella and acoustic streaming are caused by the waves from the transducer. Amplitude of these waves is controlled by the pick-to-pick voltage. This controllability allows the speed of flagellated microswimmers to be tunable by means of pick-to-pick voltage. Figure 4-9 shows the functional relationship of angular speed of flagellated rotational microswimmers and pick-to-pick voltage from 40 V_{PP} to 160 V_{PP}. As shown in Figure 4-9a, flagellum oscillation was not observed as expected. Acoustic

streaming which was caused by flagellum oscillation began instantly once the PZT transducer was turned on. Figure 4-9a-f shows a full counter clockwise rotation of a flagellated rotational microswimmer at 160 V_{PP} in 6 frames starting from zero time with no oscillation and rotation. Here, one rotation was completed in 300 milliseconds. The angular speed of rotational microswimmers increases gradually under increasing V_{PP}. As shown in Figure 4-9g, the angular speed is ~ 25 RPM at 40 V_{PP} (minimum V_{PP} in this study) rising up to ~ 200 RPM at 160 V_{PP} (maximum V_{PP} in this study) in a monotone.

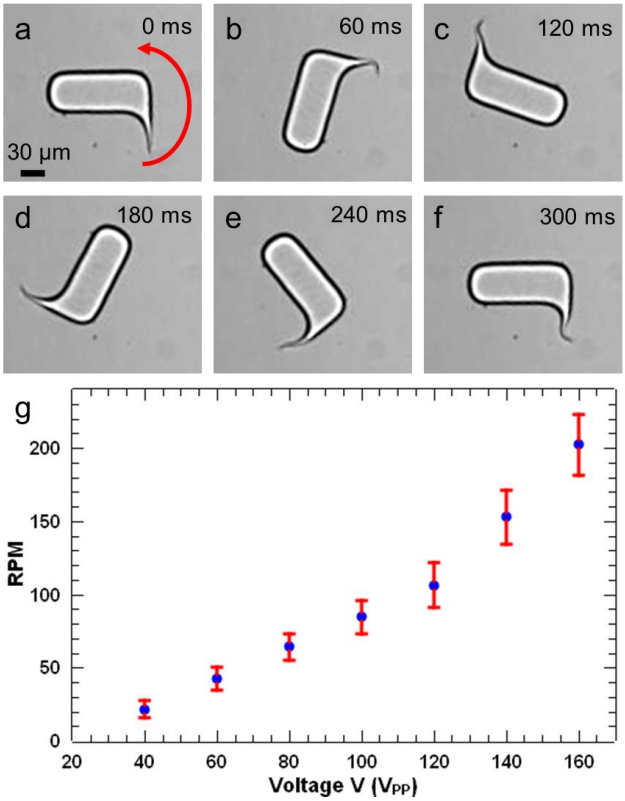

Figure 4-9 Microswimmer's rotational movement. (a), (b), (c), (d), (e) and (f) A full revolution which is divided into six frames, takes 300 ms at 160 V_{PP}. (e) Angular velocity of microswimmers in response to different values of voltage. Starting from ~ 25 RPM at 40 V_{PP}, angular velocities of rotational microswimmers increase up to ~ 200 RPM at 160 V_{PP}.

Chapter 5

5.1 Summary

We have demonstrated single step *in situ* fabrication of microrotors using UV polymerization in a microchannel. The microrotors have sharp-edge structures that are positioned asymmetrically on the rotor crossbar. Piezoelectric transducers enable acoustofluidic actuation of the microrotor through streaming flows induced by the oscillations of sharp-edge structures. These acoustic streaming flows break reflection symmetry and thus induce a net torque on the rotor arm. The angular speed increases uniformly and nearly linearly with the number of arms, attaining the highest speed for six arms. The angular speed is also controlled by the peak-to-peak voltage applied to the transducer, achieving rates above 1200 RPM for the 6-arm microrotor driven at 160 V_{PP}.

Additionally, we have demonstrated that in situ fabrication and acoustic actuation of flagellated microswimmers. Acoustically actuated flagellum was utilized to mimic biological microswimmers such as bacteria. Rotational and directional propelling of flagellated microswimmers have been characterized. For the former, we designed the microswimmers having flagella on the right side for clockwise rotation, on the left side for counter clockwise rotation. For the latter, we designed microswimmers with a head and a flagellum mimicked tail. Under acoustic field once the transducer was on, the flagella of the microswimmers began to oscillate and, thus, generate acoustic microstreaming at the end of flagella. This acoustic streaming propelled the flagellated microswimmers through

intended movements such as directional and rotational. The directional microswimmers could reach up to~1200 μm/s while rotational microswimmers could perform 200 RPM at 160 V_{PP}. Deep understanding of acoustic field and better microswimmer design could end up higher performance.

5.1 Future Recommendations

We believe that even higher performance can be obtained with further optimization of geometry and composition. The simple fabrication and easy actuation of these microrotors makes them suitable for many potential applications, such as micropumps, micromixers, microgear systems, and micromachinery in physics, biochemistry, and biomedical engineering. Their streaming on the sharp-edge structures and high rotational performance can mix multiple solutions immediately. Also, high rotation of microrotors allow them to pump the liquid inside the microchannel. Microgear system and micromachinery are also available applications to transmit the torque and power to another systems.

Additionally, microswimmers have great potential since they mimic biological microorganisms. Here, simple, durable and inexpensive fabrication as well as nontoxic, biocompatible and remote control of biologically mimicked microswimmers show the potential of them for future applications such as targeted drug delivery, particle separation, mixing, pumping, micro assembly, cell manipulation, microsurgery and chemical analysis in physics, biochemistry, and biomedical engineering. As a next step, flagellated microswimmers should be fabricated using biocompatible solutions, and controlled in

biological mediums. Then, these biologically mimicked swimmers should be used inside the body in order to do some special missions. They can be used for targeted drug delivery to transfer some medication to diseased part of the body. That improvement can allow us to use medications, which are mostly toxic to healthy tissues, only for diseased tissues. Besides, flagellated microswimmers are appropriate for microsurgery. For example, they can be moved to diseased part of the body using acoustic. Then, they can drill, trim and do microsurgery. Since acoustic is not harmful for biological cells and tissues, minimum invasion will happen.

References

[1] N. Blow, *Nat. Methods* **2009**, *6*, 683.

[2] G. M. Whitesides, *Nature* **2006**, *442*, 368.

[3] X. Ding, P. Li, S.-C. S. Lin, Z. S. Stratton, N. Nama, F. Guo, D. Slotcavage, X. Mao, J. Shi, F. Costanzo, T. J. Huang, *Lab Chip* **2013**, *13*, 3626.

[4] A. M. Streets, Y. Huang, *Biomicrofluidics* **2013**, *7*, 011302.

[5] J. M. Perkel, *Science (80-.).* **2008**, DOI 10.1126/science.opms.p0800029.

[6] G. K. Batchelor, *An Introduction to Fluid Dynamics*, Cambridge University Press, Cambridge, **2000**.

[7] H. A. Stone, A. D. Stroock, A. Ajdari, *Annu. Rev. Fluid Mech.* **2004**, *36*, 381.

[8] J. J. L. Higdon, *J. Fluid Mech.* **1979**, *90*, 685.

[9] E. M. Purcell, *Am. J. Phys.* **1977**, *45*, 3.

[10] A. C. R. Grayson, R. S. Shawgo, A. M. Johnson, N. T. Flynn, Y. Li, M. J. Cima, R. Langer, *Proc. IEEE* **2004**, *92*, 6.

[11] M. A. Unger, *Science (80-.).* **2000**, *288*, 113.

[12] A. Waldschik, S. Büttgenbach, *Microsyst. Technol.* **2010**, *16*, 1581.

[13] K. S. Ryu, K. Shaikh, E. Goluch, Z. Fan, C. Liu, *Lab Chip* **2004**, *4*, 608.

[14] W. C. Chang, D. W. Sretavan, *Clin. Neurosurg.* **2007**, *54*, 137.

[15] C. H. Ahn, M. G. Allen, in *Proc. IEEE Micro Electro Mech. Syst. 1995*, IEEE, **n.d.**, p. 408.

[16] R. Nosrati, A. Driouchi, C. M. Yip, D. Sinton, *Nat. Commun.* **2015**, *6*, 8703.

[17] L. Eamer, R. Nosrati, M. Vollmer, A. Zini, D. Sinton, *Biomicrofluidics* **2015**, *9*, 044113.

[18] J. Kim, H. L. Ennis, T. H. Nguyen, X. Zhuang, J. Luo, J. Yao, R. H. Kessin, M. Stojanovic, Q. Lin, *Sensors Actuators A Phys.* **2012**, *188*, 312.

[19] S. Rozhok, C.-F. Shen, P.-L. Littler, Z. Fan, C. Liu, C. Mirkin, R. Holz, *Small* **2005**, *1*, 445.

[20] Y. Xie, D. Ahmed, M. I. Lapsley, S.-C. S. Lin, A. A. Nawaz, L. Wang, T. J. Huang, *Anal. Chem.* **2012**, *84*, 7495.

[21] A. J. Chung, D. Kim, D. Erickson, *Lab Chip* **2008**, *8*, 330.

[22] Y. Kim, J. Lee, S. Kwon, *J. Micromechanics Microengineering* **2009**, *19*, 105028.

[23] Liang-Hsuan Lu, Kee Suk Ryu, Chang Liu, *J. Microelectromechanical Syst.* **2002**, *11*, 462.

[24] M. Sen, D. Wajerski, M. Gad-el-Hak, *J. Fluids Eng.* **1996**, *118*, 624.

[25] S. G. Darby, M. R. Moore, T. A. Friedlander, D. K. Schaffer, R. S. Reiserer, J. P. Wikswo, K. T. Seale, *Lab Chip* **2010**, *10*, 3218.

[26] Y. Hatwalne, S. Ramaswamy, M. Rao, R. A. Simha, *Phys. Rev. Lett.* **2004**, *92*, 118101.

[27] A. Tokarev, A. Aprelev, M. N. Zakharov, G. Korneva, Y. Gogotsi, K. G. Kornev, *Rev. Sci. Instrum.* **2012**, *83*, 065110.

[28] B.-U. Moon, S. S. H. Tsai, D. K. Hwang, *Microfluid. Nanofluidics* **2015**, *19*, 67.

[29] T. Yue, M. Nakajima, M. Takeuchi, T. Fukuda, T. Fuku, *Int. J. Adv. Robot. Syst.* **2014**, *11*, 1.

[30] T. Yue, M. Nakajima, M. Ito, M. Kojima, T. Fukuda, in *2011 IEEE/RSJ Int. Conf. Intell. Robot. Syst.*, IEEE, **2011**, pp. 433–438.

[31] A. Sokolov, M. M. Apodaca, B. A. Grzybowski, I. S. Aranson, *Proc. Natl. Acad. Sci.* **2010**, *107*, 969.

[32] R. Di Leonardo, L. Angelani, D. Dell'Arciprete, G. Ruocco, V. Iebba, S. Schippa, M. P. Conte, F. Mecarini, F. De Angelis, E. Di Fabrizio, *Proc. Natl. Acad. Sci.* **2010**, *107*, 9541.

[33] Y. Hiratsuka, M. Miyata, T. Tada, T. Q. P. Uyeda, *Proc. Natl. Acad. Sci.* **2006**, *103*, 13618.

[34] G. Loget, A. Kuhn, *Nat. Commun.* **2011**, *2*, 535.

[35] A. Nourhani, P. E. Lammert, V. H. Crespi, A. Borhan, *Phys. Fluids* **2015**, *27*, 012001.

[36] R. J. Shilton, N. Glass, S. Langelier, P. Chan, L. Y. Yeo, J. R. Friend, in (Eds: S. Juodkazis, M. Gu), **2011**, p. 82041J.

[37] R. J. Shilton, N. R. Glass, P. Chan, L. Y. Yeo, J. R. Friend, *Appl. Phys. Lett.* **2011**, *98*, 254103.

[38] D. Ahmed, M. Lu, A. Nourhani, P. E. Lammert, Z. Stratton, H. S. Muddana, V. H. Crespi, T. J. Huang, *Sci. Rep.* **2015**, *5*, 9744.

[39] M. Mijalkov, G. Volpe, *Soft Matter* **2013**, *9*, 6376.

[40] G. Grosjean, G. Lagubeau, A. Darras, M. Hubert, G. Lumay, N. Vandewalle, *Sci. Rep.* **2015**, *5*, 16035.

[41] N. Bertin, T. A. Spelman, O. Stephan, L. Gredy, M. Bouriau, E. Lauga, P. Marmottant, *Phys. Rev. Appl.* **2015**, *4*, 064012.

[42] G. Volpe, I. Buttinoni, D. Vogt, H.-J. Kümmerer, C. Bechinger, *Soft Matter* **2011**, *7*, 8810.

[43] X. Yan, Q. Zhou, J. Yu, T. Xu, Y. Deng, T. Tang, Q. Feng, L. Bian, Y. Zhang, A. Ferreira, L. Zhang, *Adv. Funct. Mater.* **2015**, *25*, 5333.

[44] M. M. Stanton, C. Trichet-Paredes, S. Sánchez, *Lab Chip* **2015**, *15*, 1634.

[45] R. W. Carlsen, M. R. Edwards, J. Zhuang, C. Pacoret, M. Sitti, *Lab Chip* **2014**, *14*, 3850.

[46] J. Simmchen, J. Katuri, W. E. Uspal, M. N. Popescu, M. Tasinkevych, S. Sánchez, *Nat. Commun.* **2016**, *7*, 10598.

[47] L. Zhang, K. E. Peyer, B. J. Nelson, *Lab Chip* **2010**, *10*, 2203.

[48] K. E. Peyer, L. Zhang, B. J. Nelson, *Nanoscale* **2013**, *5*, 1259.

[49] R. W. Carlsen, M. Sitti, *Small* **2014**, *10*, 3831.

[50] S. Ahmed, W. Wang, L. O. Mair, R. D. Fraleigh, S. Li, L. A. Castro, M. Hoyos, T. J. Huang, T. E. Mallouk, *Langmuir* **2013**, *29*, 16113.

[51] M. M. Stanton, J. Simmchen, X. Ma, A. Miguel-López, S. Sánchez, *Adv. Mater. Interfaces* **2016**, *3*, n/a.

[52] W. Gao, J. Wang, *Nanoscale* **2014**, *6*, 10486.

[53] W. Wang, W. Duan, A. Sen, T. E. Mallouk, *Proc. Natl. Acad. Sci.* **2013**, *110*, 17744.

[54] W. Wang, W. Duan, S. Ahmed, A. Sen, T. E. Mallouk, *Acc. Chem. Res.* **2015**, *48*, 1938.

[55] S. Ahmed, D. T. Gentekos, C. A. Fink, T. E. Mallouk, *ACS Nano* **2014**, *8*, 11053.

[56] J. Elgeti, R. G. Winkler, G. Gompper, *Reports Prog. Phys.* **2015**, *78*, 056601.

[57] J. Katuri, K. D. Seo, D. S. Kim, S. Sánchez, *Lab Chip* **2016**, DOI 10.1039/C6LC90022D.

[58] W. Zhu, J. Li, Y. J. Leong, I. Rozen, X. Qu, R. Dong, Z. Wu, W. Gao, P. H. Chung, J. Wang, S. Chen, *Adv. Mater.* **2015**, *27*, 4411.

[59] K. E. Peyer, S. Tottori, F. Qiu, L. Zhang, B. J. Nelson, *Chem. - A Eur. J.* **2013**, *19*, 28.

[60] J. F. Jikeli, L. Alvarez, B. M. Friedrich, L. G. Wilson, R. Pascal, R. Colin, M. Pichlo, A. Rennhack, C. Brenker, U. B. Kaupp, *Nat. Commun.* **2015**, *6*, 7985.

[61] E. Lauga, T. R. Powers, *Reports Prog. Phys.* **2009**, *72*, 096601.

[62] E. Lauga, C. Eloy, *J. Fluid Mech.* **2013**, *730*, R1.

[63] W. Wang, W. Duan, S. Ahmed, T. E. Mallouk, A. Sen, *Nano Today* **2013**, *8*, 531.

[64] T. Qiu, T.-C. Lee, A. G. Mark, K. I. Morozov, R. Münster, O. Mierka, S. Turek, A. M. Leshansky, P. Fischer, *Nat. Commun.* **2014**, *5*, 5119.

[65] W. Wang, W. Duan, Z. Zhang, M. Sun, A. Sen, T. E. Mallouk, *Chem. Commun.* **2015**, *51*, 1020.

[66] P. Dhar, Y. Cao, T. Kline, P. Pal, C. Swayne, T. M. Fischer, B. Miller, T. E. Mallouk, A. Sen, T. H. Johansen, *J. Phys. Chem. C* **2007**, *111*, 3607.

[67] A. Ghosh, P. Fischer, *Nano Lett.* **2009**, *9*, 2243.

[68] W. Wang, S. Li, L. Mair, S. Ahmed, T. J. Huang, T. E. Mallouk, *Angew. Chemie* **2014**, *126*, 3265.

[69] Y. Chen, X. Ding, S.-C. Steven Lin, S. Yang, P.-H. Huang, N. Nama, Y. Zhao, A. A. Nawaz, F. Guo, W. Wang, Y. Gu, T. E. Mallouk, T. J. Huang, *ACS Nano* **2013**, *7*, 3306.

[70] J. Feng, J. Yuan, S. K. Cho, *Lab Chip* **2015**, *15*, 1554.

[71] S. E. Chung, J. Kim, S.-E. E. Choi, L. N. Kim, S. Kwon, *J. Microelectromechanical Syst.* **2011**, *20*, 785.

[72] S. E. Chung, W. Park, H. Park, K. Yu, N. Park, S. Kwon, *Appl. Phys. Lett.* **2007**, *91*, 041106.

[73] H. Kim, J. Ge, J. Kim, S. Choi, H. Lee, H. Lee, W. Park, Y. Yin, S. Kwon, *Nat. Photonics* **2009**, *3*, 534.

[74] H. Wang, Z. Liu, S. Kim, C. Koo, Y. Cho, D.-Y. Jang, Y.-J. Kim, A. Han, *Lab Chip* **2014**, *14*, 947.

[75] D. Ahmed, A. Ozcelik, N. Bojanala, N. Nama, A. Upadhyay, Y. Chen, W. Hanna-Rose, T. J. Huang, *Nat. Commun.* **2016**, *7*, 11085.

[76] P.-H. Huang, N. Nama, Z. Mao, P. Li, J. Rufo, Y. Chen, Y. Xie, C.-H. Wei, L. Wang, T. J. Huang, *Lab Chip* **2014**, *14*, 4319.

[77] D. Ahmed, X. Peng, A. Ozcelik, Y. Zheng, T. J. Huang, *AIP Adv.* **2015**, *5*, 097161.

[78] D. Ahmed, H. S. Muddana, M. Lu, J. B. French, A. Ozcelik, Y. Fang, P. J. Butler, S. J. Benkovic, A. Manz, T. J. Huang, *Anal. Chem.* **2014**, *86*, 11803.

[79] P.-H. Huang, Y. Xie, D. Ahmed, J. Rufo, N. Nama, Y. Chen, C. Y. Chan, T. J. Huang, *Lab Chip* **2013**, *13*, 3847.

[80] A. Ozcelik, D. Ahmed, Y. Xie, N. Nama, Z. Qu, A. A. Nawaz, T. J. Huang, *Anal. Chem.* **2014**, *86*, 5083.

[81] D. Dendukuri, P. Panda, R. Haghgooie, J. M. Kim, T. A. Hatton, P. S. Doyle, *Macromolecules* **2008**, *41*, 8547.

[82] D. C. Pregibon, M. Toner, P. S. Doyle, *Langmuir* **2006**, *22*, 5122.

[83] P. Panda, S. Ali, E. Lo, B. G. Chung, T. A. Hatton, A. Khademhosseini, P. S. Doyle, *Lab Chip* **2008**, *8*, 1056.

[84] M. Li, M. Humayun, J. a. Kozinski, D. K. Hwang, *Langmuir* **2014**, *30*, 8637.

[85] C. Decker, a D. Jenkins, *Macromolecules* **1985**, *18*, 1241.

[86] N. Nama, P.-H. Huang, T. J. Huang, F. Costanzo, *Lab Chip* **2014**, *14*, 2824.

[87] N. Nama, R. Barnkob, Z. Mao, C. J. Kähler, F. Costanzo, T. J. Huang, *Lab Chip* **2015**, *15*, 2700.

[88] J. Vanneste, O. Bühler, *Proc. R. Soc. London A Math. Phys. Eng. Sci.* **2011**, *467*, 1779.